Modular Enhancement of Melatonin Pathway by Evolutionary Optimization of Tryptophan Biosynthesis and AtCOMT Catalytic Function

Yijun Liu, Ziyu Wang, Wenbo Nie, Yupeng Zhai, Zhaokun Jiang, Wenrui Wang, Daoyu Xie, Xiao Liu, Tongtong Lang, Rui Jiang, Jiani Xiao, Xi Jiang, Xin Li, Pengchao Wang

Abstract:

Melatonin (MT), a ubiquitous circadian rhythm regulator, faces increasing global demand. However, its production through conventional methods is hindered by high cost, complexity, and low yield. These limitations pose significant challenges for both basic research and large-scale applications. In this study, the catalytic efficiency of *Arabidopsis thaliana* caffeic acid O-methyltransferase (AtCOMT) in MT biosynthesis was enhanced through systematic optimization of L-tryptophan (L-Trp) synthesis and utilization, combined with enzyme engineering through directed evolution. This study enhanced melatonin precursor tryptophan production to 3.99g/L via upstream genes knockout, overexpression, whole-genome mutagenesis, and *tnaC*-biosensor screening, achieving a 1609.9-fold increase over the wild-type BW25113. We developed a growth-coupled high-throughput screening system using a synthetic methyl cycle to

select AtCOMT mutants. The best variant exhibited 84% higher catalytic efficiency than the highest literature value, demonstrating the power of integrating directed evolution, biosensors, and computational design for melatonin biosynthesis.

Keywords: melatonin; whole cell biosensor; whole genome mutation; pathway optimization; directed evolution

1.Introduction

Melatonin (MT) is an evolutionarily conserved molecule that acts as a crucial regulator of circadian rhythms widely present in animals, plants, and microorganisms[1,2]. With growing global demand, conventional production methods, such as chemical synthesis and extraction from plants or animal sources, are associated with environmental, safety, and economic concerns[3,4]. Microbial cell factories have emerged as a sustainable and cost-effective alternative, with fermentation costs estimated to be only about one-tenth of those of chemical synthesis[5,6]. However, the biosynthetic pathway for melatonin production from L-tryptophan (L-Trp) still challenged by two major bottlenecks: limited precursor supply through the shikimate pathway and low catalytic efficiency of key enzymes[7,8].

Previous studies have independently shown that L-tryptophan flux can be enhanced by either using an engineered chassis strain (BW-RT, lacking the *trpR*

repressor and *tnaAB* degradation genes) or by introducing a plasmid (pBR322-trpfbrEDCBA-aroGfbr-serAfbr) that overexpresses feedback-resistant versions of the trp operon and key precursor pathway genes, thereby increasing catalytic capacity and overcoming allosteric regulation[9,10]. Moreover, subjecting the strain to genome-wide evolutionary pressure using a tryptophan biosensor to uncover adaptive mutations beyond rational design represents a critical and unaddressed step. The final methylation step driven by AtCOMT is a bottleneck. While a mutant with 9.5-fold higher activity has been reported, its performance is still insufficient[11].

Directed evolution, leveraging the power of genetic diversity and selection, is widely employed to engineer proteins or enzymes with enhanced or novel functions[12]. Furthermore, whole-cell biosensors represent an efficient screening tool by directly coupling enzyme activity to bacterial growth[13].

In this study, we implemented an integrated strategy to enhance the supply of melatonin biosynthetic precursors by combining rational strain design with genome-wide mutagenesis to boost L-Trp production in *E. coli*. We also used a cysteine auxotrophic whole-cell biosensor that couples AtCOMT activity to bacterial growth, enabling high-throughput screening of functional mutants to improve the catalytic efficiency of the final methylation step[14]. By integrating rational design, directed evolution, whole-genome sequencing, and molecular docking, our work provides a

blueprint for an innovative strategy for systematically optimizing the melatonin biosynthetic pathway.

2. Result

2.1 Rational Design Evolution to produce high L-Tryptophan bacterial strains

To establish a robust platform for MT synthesis, we first aim to build a chassis *E. coli* strain by optimizing the production of L-tryptophan, the essential precursor of MT. This was achieved by a two-stage rational design approach: combinatorial screening, followed by the targeted elimination of competing metabolic pathways (branches).

2.1.1. Combinatorial Screening Identifies an Optimal Chassis Strain with High-Yield Plasmids

In this study, six distinct chassis strains and three plasmids were constructed **(Table 1)**. The plasmids were designed to incrementally remove bottlenecks in the tryptophan pathway: pTRP1 expresses the wild-type trp operon; pTRP2 contains an S40F point mutation in *trpE* to alleviate feedback inhibition from tryptophan; and based on pTRP2, further incorporates feedback-resistant variants of key precursor pathway genes—*aroG* and *serA*—to enhance metabolic flux[10]. To systematically evaluate production performance, each plasmid was individually transformed into three engineered chassis strains with distinct genetic backgrounds: the wild-type BW25113

(BW), a *trpR* knockout derivative (BW-R)[15] to abolish transcriptional repression, and a double-knockout strain deficient in both *trpR* and the tryptophan degradation genes *tnaAB* (BW-RT)[9]. The combinatorial screen revealed that plasmid pTRP3 conferred the highest L-tryptophan production performance among all chassis strains **(Figure 1B)**. The optimal combination was the BW-RT strain harboring pTRP3, which achieved a titer of 2.997 g/L. This result highlighted the effectiveness of a synergistic engineering strategy—including transcriptional deregulation, disruption of tryptophan degradation, and incorporation of feedback-resistant biosynthetic enzymes.

Identifier	Category	Description/Genotype
BW	Strain	*E. coli* BW25113
BW-R	Strain	BWΔ*trpR*
BW-RT	Strain	BWΔ*trpR*Δ*tnaAB*
BW-RTG	Strain	BWΔ*trpR*Δ*tnaAB*Δ*ptsG*
BW-RTF	Strain	BWΔ*trpR*Δ*tnaAB*Δ*pykF*
BW-RTA	Strain	BWΔ*trpR*Δ*tnaAB*Δ*pykA*
BW-RTP	Strain	BWΔ*trpR*Δ*tnaAB*Δ*pheA*
pTRP1	Plasmid	pYB1a-P23119-*trpEDCBA*
pTRP2	Plasmid	pYB1a-P23119-*trpE*^{S40F}*DCBA*
pTRP3	Plasmid	pBR322-*trp*^{fbr}*EDCBA-aroG*^{fbr}*-serA*^{fbr}

Table 1. Plate strain and plasmid identifier.

2.1.2. Redirecting Carbon Fluxes via Knockout of Competing Pathways

Based on the optimal combination BW-RT (pTRP3) strain, we next sought to direct more carbon metabolic fluxes towards the L-tryptophan synthesis pathway. We identified four key competitive nodes in the central metabolic pathway and conducted gene knockouts: the *ptsG* gene responsible for major glucose uptake but consuming the

precursor PEP[16,17], the *pykF* and *pykA* genes that catalyze the conversion of PEP to pyruvate[18,19], and the *pheA* gene that catalyzes the diversion of branch acid to the phenylalanine synthesis pathway[20]. Individual knockout of these genes in the BW-RW (pTRP3) background revealed that removing the *pheA* gene had the most significant enhancement on L-tryptophan production **(Figure 1C)**. The final engineered strain, BW-RTP (BWΔ*trpR*Δ*tnaAB*Δ*pheA)* equipped with the pTRP3 plasmid, reached an L-tryptophan yield of 3.99 g/L, achieving a 1609.9-fold increase over its parent strain (BW) Compared with the parent strain (equipped with the same plasmid), the yield was increased by 22.8%.

2.2 Construction of Tryptophan Biosensors and Screening of Mutants

Built upon the rational design, we further implemented a directed evolution strategy using genome-wide random mutagenesis coupled with a high-throughput biosensor screening platform.

2.2.1 Development and Validation of a TnaC-Based Tryptophan Biosensor

To enable high-throughput screening of L-tryptophan high-yielding strains, a biosensor was constructed using the tryptophan operon leader peptide *tnaC*, which regulates the expression of an *mCherry* reporter in response to intracellular L-tryptophan concentrations (pLB1s-PBAD-*tnaC*-*mCherry*-*Cmr*)[21]. At low tryptophan concentrations, RF2-mediated translation termination and Rho-dependent transcription

termination occur, conversely, high intracellular tryptophan causes ribosome stalling, which prevents Rho binding and thereby enables transcription of the downstream reporter genes **(Figure 2A)**. Under tryptophan concentrations ranging from 0 to 1.5 g/L, growth improved proportionally with Trp supplementation **(Figure 2B)**. Within this range, the BWΔ*trpR*Δ*tnaAB*-pYB1a-P23119-*tnaE*^{S40F}*DCBA* strain was selected for directed evolution.

A high-throughput random mutagenesis plasmid, MP6, and the *TnaC-based* biosensor were engineered to generate a library of *Escherichia coli* mutants through expression of a protein that impairs DNA replication fidelity, thereby increasing whole genome mutation frequency[22]. The plasmid employs the arabinose-inducible promoter, enabling regulated expression of the mutagenesis-enabling gene through the addition of arabinose **(Figure 2C)**. The chassis strain BWΔ*trpR*Δ*tnaAB* was co-transformed with plasmids MP6-K, pLB1s-PBAD-*tnaC-mCherry-Cmr*, and pYB1a-P23119-*tnaE*^{S40F}*DCBA*.

After ten rounds of evolution and screening **(Figure 2D)**, two mutants, 3-4 and 10-7, exhibited tryptophan production approximately 3.25 times higher than the wild-type strain **(Figure 2D)**. Subsequent replicate fermentations in enlarged 15 mL confirmed that strains 3-4 and 10-7 showed the most pronounced improvement in Trp yield. Therefore, they were selected for whole-genome resequencing **(Figure 2E)**.

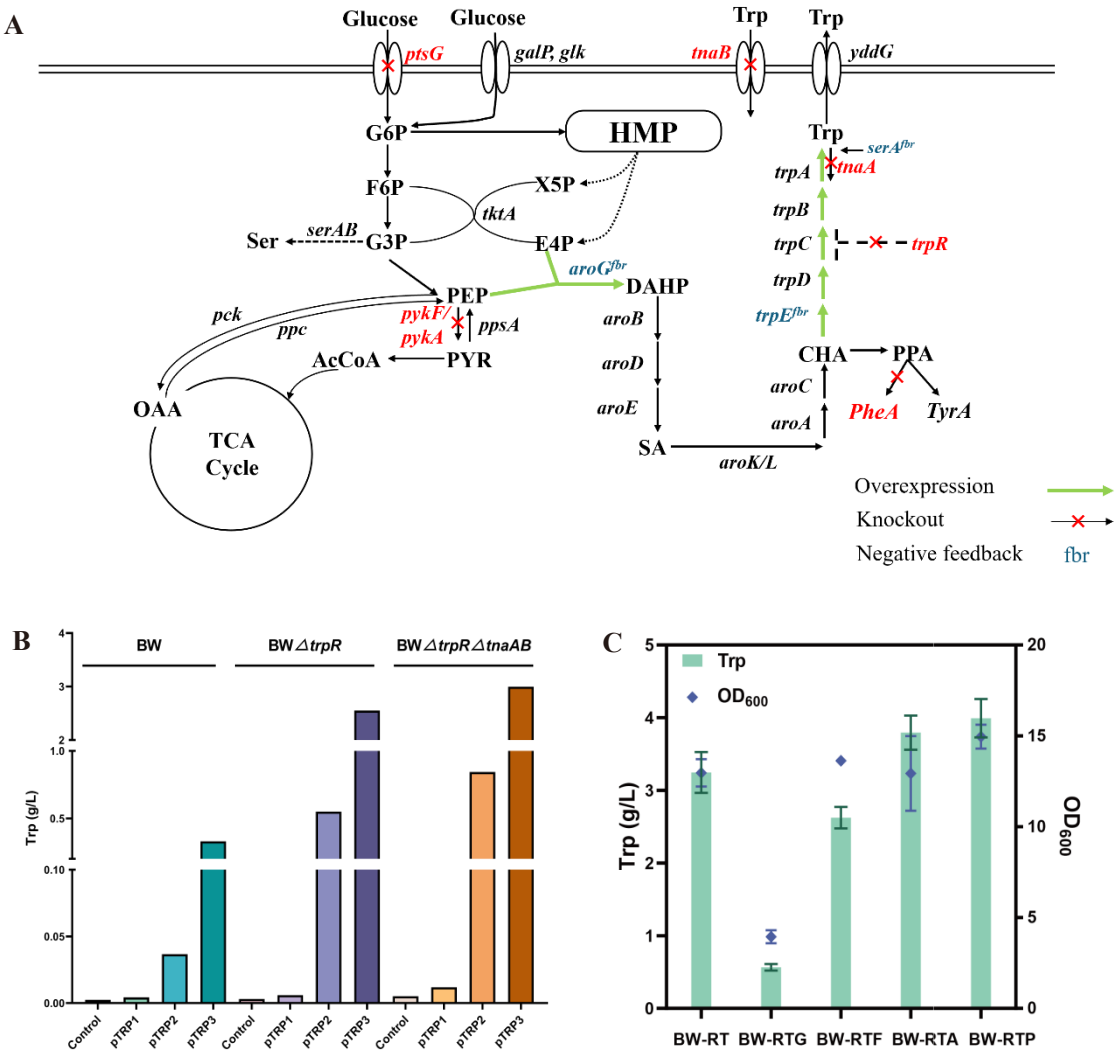

Figure 1. Metabolic pathway optimization of trp strains.

(A) Schematic diagram of L-tryptophan biosynthesis and related central metabolic networks in *Escherichia coli*. Genes that were overexpressed or knocked out to enhance L-tryptophan synthesis are indicated in red font. Dashed arrows represent multi-step reactions or omitted reaction pathways. **(B)** Comparison of L-tryptophan production across different host strains and plasmid combinations. Plasmids pTRP1, pTRP2, pTRP3 and the empty plasmid control were respectively introduced into strains BW, BW-R and BW-RT for shake flask fermentation. **(C)** Effects of knocking out key metabolic node genes (*pstG, pykF, pykA, pheA*) on L-tryptophan production and cell growth (OD600) in the BW-RT strain background. All tested strains in the figure were equipped with the high-yield plasmid pTRP3. Data are presented as mean ± standard deviation (n=3). Note: All strains in Figure C were transformed with the pTRP3 plasmid.

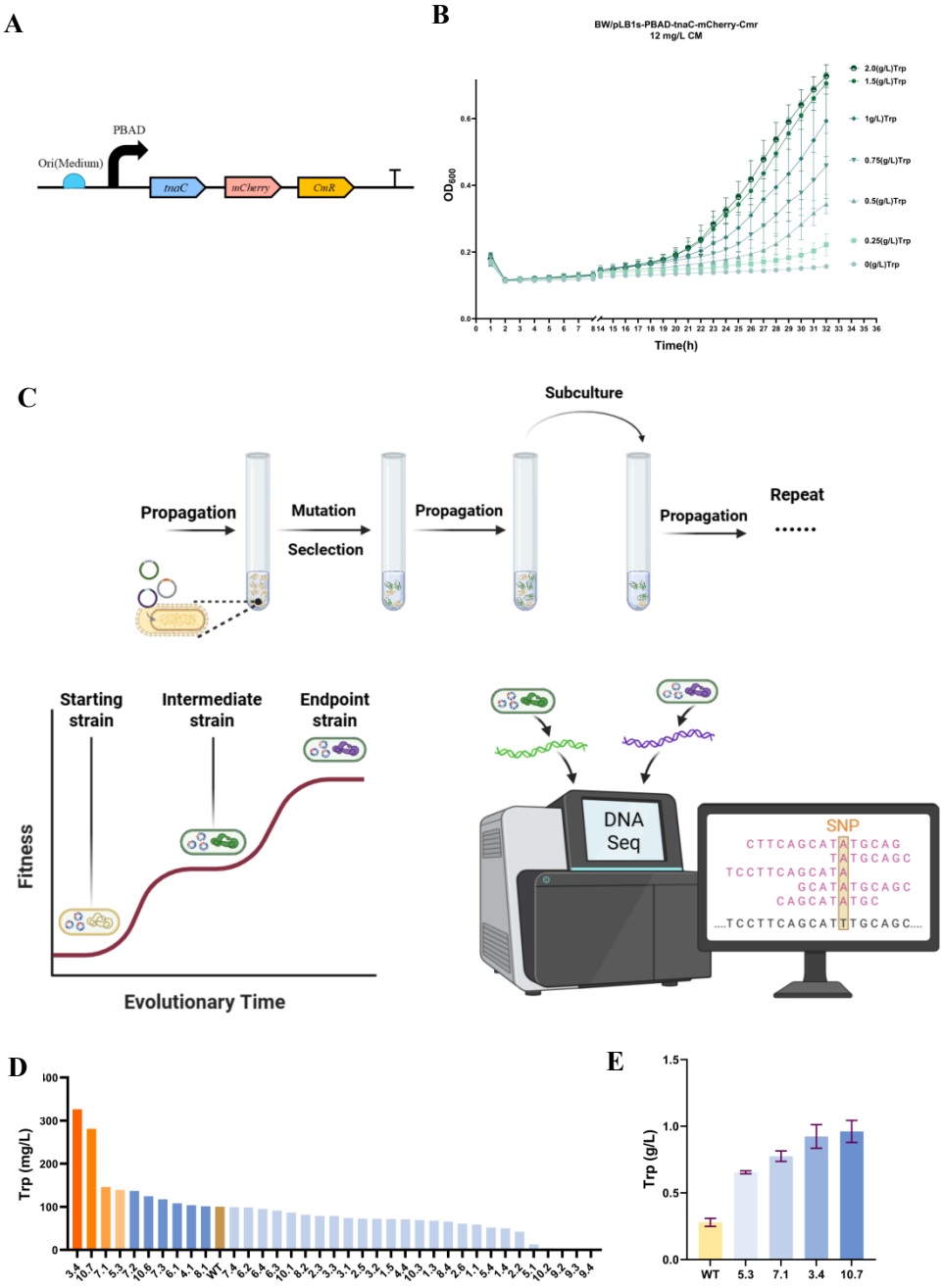

Figure 2. Construction of the *TnaC-based* tryptophan biosensor and irrational design based on the MP6 mutagenesis plasmid.

(A) Genetic circuit of the biosensor plasmid pLB1s-PBAD-*tnaC-mCherry-Cmr*. **(B)** Dose-dependent enhancement of bacterial growth with increasing tryptophan concentrations (0–1.5 g/L). **(C)** The MP6 plasmid enables genome-wide random mutagenesis upon arabinose induction. High-producing strains were initially screened using the tryptophan biosensor, validated by HPLC for production yield, and subsequently subjected to whole-genome resequencing analysis. **(D)** Preliminary HPLC analysis indicated that mutant strains 3-4 and 10-7 exhibited the highest

tryptophan production. **(E)** Repeated fermentation validation confirmed that mutants 10-7 and 3-4 showed a significant increase in tryptophan yield, reaching approximately three times that of the wild-type strain.

2.2.2 Analysis of whole genome mutation results

2.2.2.1 Identification and Comparison of Genomic Variations

Whole-genome sequencing of the top-performing strains revealed a large number of mutations, predominantly single nucleotide polymorphisms (SNPs) C→T transitions, broadly distributed across the chromosome **(Figure 3A and 3C)**. Directed evolution results in substantial genomic changes, with SNPs increasing from 60 in strain 3-4 to 175 in strain 10-7 **(Figure 3A)**. Strains 3-4 and 10-7 shared 29 SNPs, while 25 were unique to 3-4 and 140 were unique to 10-7 **(Figure 3B)**, indicating convergent and divergent evolutionary trajectories toward the high-yield phenotype.

2.2.2.2 Functional Enrichment Analysis Reveals Divergent Evolutionary Strategies

Functional enrichment analyses elucidate the molecular basis of the evolutionary strategies of the high-yield strains. Gene Ontology (GO) analysis of shared mutations shows significant enrichment in tryptophan and aromatic amino acid biosynthesis, confirming that mutations targeted and enhanced the biosynthesis pathway **(Figure 3D).** The unique mutations pointed to distinct mechanisms. In strain 3-4, mutations were enriched in RNA metabolism and related processes, indicating enhanced regulatory networks for information processing and metabolic control **(Figure 3E)**. In contrast,

unique mutations in strain 10-7 predominated in membrane-associated processes, such as biogenesis and transport **(Figure 3F)**.

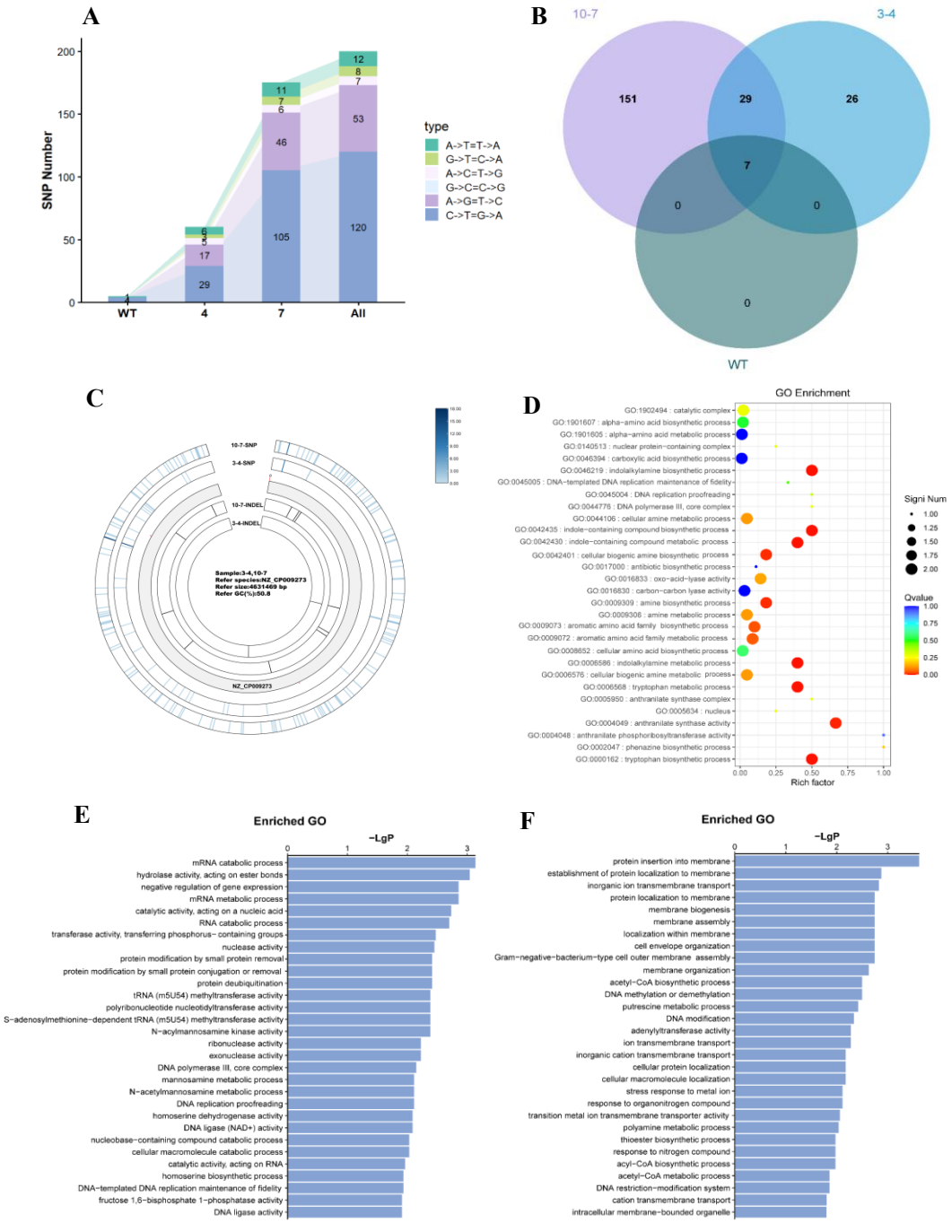

Figure 3. Mutation characteristics and functional enrichment analysis of evolved strains.

(A) Bar chart of SNP counts by mutation type (legend). Total SNPs increase from 60 in strain 3-4

to 175 in strain 10-7, with C→T transitions predominant, consistent with mutational bias in directed evolution. **(B)** Venn diagram of shared and unique SNPs: strains 3-4 and 10-7 share 29 SNPs, with 25 unique to 3-4 and 140 unique to 10-7, revealing divergent adaptive trajectories toward the high-yield phenotype. **(C)** Circos plot of chromosomal mutation distribution. Mutations disperse broadly, indicating non-localized adaptive changes. Concentric tracks (outermost to innermost): (i) SNP density in strain 10-7; (ii) SNP density in strain 3-4; (iii) InDel positions in strain 10-7; (iv) InDel positions in strain 3-4. All tracks use a heatmap-style color scale, where color intensity represents local variant density in 5-kb genomic windows (darker shades indicate higher counts). **(D)** Gene Ontology (GO) enrichment for genes with shared mutations in both evolved strains (3-4 and 10-7). Bubble plot of top enriched GO terms: The x-axis shows the Rich factor (enrichment level); bubble size represents gene count per term; the color scale denotes Q-value (adjusted P-value), with red indicating lower Q-values (higher significance). **(E)** Horizontal bar chart of top enriched GO terms for unique mutations in strain 3-4. Bar length corresponds to $-\log^{10}$ (P-value), with longer bars denoting higher significance. Enriched terms include RNA/mRNA metabolism, negative regulation of gene expression, and DNA replication proofreading. **(F)** Horizontal bar chart (as in B) of top enriched GO terms for unique mutations in strain 10-7. Enriched terms center on membrane and envelope functions, including protein insertion into membrane, membrane biogenesis, and inorganic ion transmembrane transport.

2.2.2.3 Gene-Level Strategies for Tryptophan Production

Shared mutations in *trpD* and *trpE* likely enhance flux through the core biosynthetic pathway. Mutations in strain 3-4 (*ligA* and *pnp*) potentially increase NADPH availability and degrade competing pathway mRNAs, respectively, supporting regulatory network enhancements. In contrast, mutations in strain 10-7 (*rhtC* and *tyrR*) facilitate aromatic amino acid efflux and derepression of shikimate pathway genes, promoting transport robustness. Roles are inferred from mutational analysis and prior

studies[23,24,25,26,27]; functional validation is recommended **(Table 2)**.

Additional candidate genes appear in **Supplementary Table 1**.

Strain (Both/3-4, 10-7)	Functional Category	Gene	Potential Role in Tryptophan Overproduction	Reference
Both	Tryptophan synthesis	*trpD*	Increase enzyme activity	22
Both	Tryptophan synthesis	*trpE*	Increase enzyme activity	22
3-4	Global Regulation	*ligA*	Increases NADPH availability via enhanced NAD^+ cycling	23
3-4	Global Regulation	*pnp*	Degrades competing pathway mRNAs	24
10-7	Transport & Export	*rhtC*	Exports aromatic amino acids, potentially reducing feedback inhibition	25
10-7	Precursor Supply	*tyrR*	Relieves transcriptional repression of the upstream shikimate pathway	26

Table 2. Key gene mutations and their potential roles in tryptophan overproduction.

GO analyses identify shared mutations in tryptophan biosynthesis genes *trpD* and *trpE*, enhancing core pathway flux. Unique mutations in strain 3-4 potentially increase reducing power (*ligA*) and degrade competing pathway mRNAs (*pnp*), whereas those in strain 10-7 promote amino acid efflux (*rhtC*) and precursor supply (*tyrR*).

2.3 Construction of MT Synthetic pathway and Identification of Rate Limiting Steps

With a high-yielding L-Trp producing *E. coli* strain, next, we established a heterologous four-enzyme biosynthetic pathway to convert L-Trp to melatonin **(Figure 4A)**.

2.3.1 Individual Enzyme Activity Assays Identified AtCOMT as the Bottleneck

We analyzed the catalytic efficiencies of the four enzymes individually: *Dugesia*

japonica tryptophan hydroxylase (DjTPH), *Catharanthus roseus* Tryptophan Decarboxylase (CrTDC), *S. griseofuscus* arylalkylamine N-acetyltransferase (SgAANAT), and *Arabidopsis thaliana* caffeic acid O-methyltransferase (AtCOMT)[28,29,30,31]. Results indicated that AtCOMT was the primary rate-limiting enzyme, which exhibited a substantially low substrate conversion rate of only 0.5% in 12h **(Figure 4B)**. Therefore, AtCOMT was identified as the primary target for directed evolution to enhance its enzymatic activity.

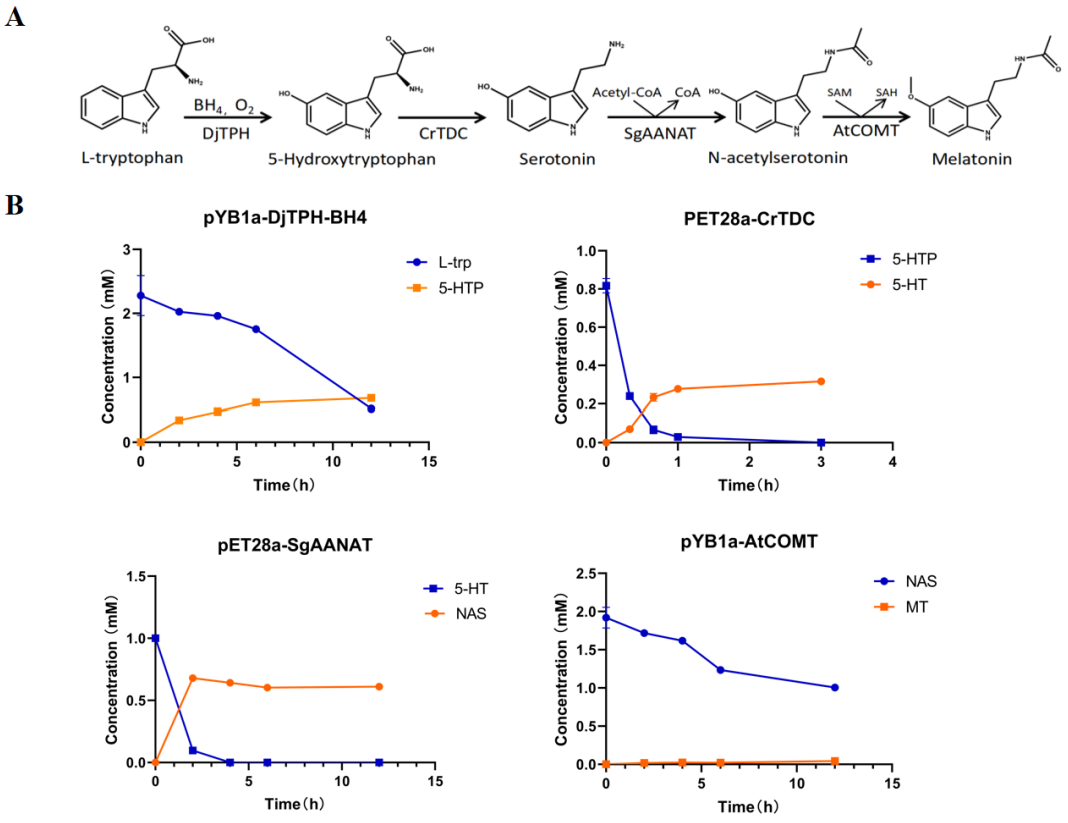

Figure 4. The synthesis pathway from tryptophan to melatonin and the detection of single enzyme activity.

(A) The melatonin biosynthesis pathway. DjTPH, tryptophan hydroxylase; CrTDC, tryptophan decarboxylase; SgAANAT, serotonin N-acetyltransferase; AtCOMT, caffeic O-methyltransferase; SAM, S-adenosylmethionine; SAH, S-adenosylhomocysteine. **(B)** Single enzyme activity assays

revealed that DjTPH had a conversion rate of 41.2% in 12h; CrTDC had a conversion rate of 43.8% in 3 hours; SgAANAT had a conversion rate of 65.1% in 12h; AtCOMT had a conversion rate of only 0.5% in 12h.

2.4 Directed Evolution of AtCOMT for Enhanced Catalytic Efficiency

Given the minimal enzymatic activity of AtCOMT, a directed evolution library was screened through a high-throughput biosensor platform.

2.4.1 Construction and Verification of a Cysteine Biosensor for AtCOMT Activity

To facilitate screening of AtCOMT variants, we constructed a cysteine deficiency biosensor by coupling AtCOMT activity to *Escherichia coli* growth[14]. In this system, bacterial viability relies on AtCOMT-mediated conversion of S-adenosylmethionine (SAM) to S-adenosylmethionine (SAH), an important precursor for cysteine synthesis **(Figure 5A and 5B)**. The growth of *CysE* gene-knockout bacterial strains depends either on the functional expression of the *Cys3* and *Cys4* genes to synthesize cysteine or on an external supply of cysteine. Sensor validation via exogenous cysteine supplementation showed dose-dependent restoration of growth, with complete absence in cysteine-free controls **(Figure 5C)**, confirming a functional whole-cell biosensor. Comparison between wild-type AtCOMT and a known high-activity AtCOMT mutant C296F-Q310L-V314T (AtCOMT***) revealed that the mutant strain reached approximately five-fold higher optical density after 50 hours **(Figure 5D)**, demonstrating the sensor's capability for enzyme activity screening and providing a

reliable platform for AtCOMT activity screening.

2.4.2 Selection of AtCOMT Mutants Using a Whole-Cell Biosensor

Following confirmation of the cysteine auxotrophic biosensor's functional validity, We screened a mutant library of *AtCOMT* generated by error-prone PCR, based on a known AtCOMT*** mutant C296F-Q310L-V314T that exhibits 9.5-fold higher enzymatic activity[11]. A large number of *AtCOMT* fragments harboring 2–3 missense mutation sites were assembled into the pYB1a vector via Golden Gate ligation and subsequently transformed into *Escherichia coli* DH5α. Mixed bacterial plasmids were then extracted and transformed into the cysteine auxotrophic chassis strain BWΔ*CysE*-PLB1s-*Cys3*-*Cys4*, followed by biosensor-mediated screening of bacteria with growth advantages **(Figure 5E)**. In the experiment, the obtained mixed bacterial cells were first cultured in M9 medium supplemented with exogenous cysteine for transition. Once slight turbidity was observed, the culture was transferred at a 5% inoculum ratio to cysteine-free M9 medium containing S-adenosylmethionine (SAM) and N-acetylserotonin (NAS) for further cultivation. This process was repeated upon reoccurrence of slight turbidity.

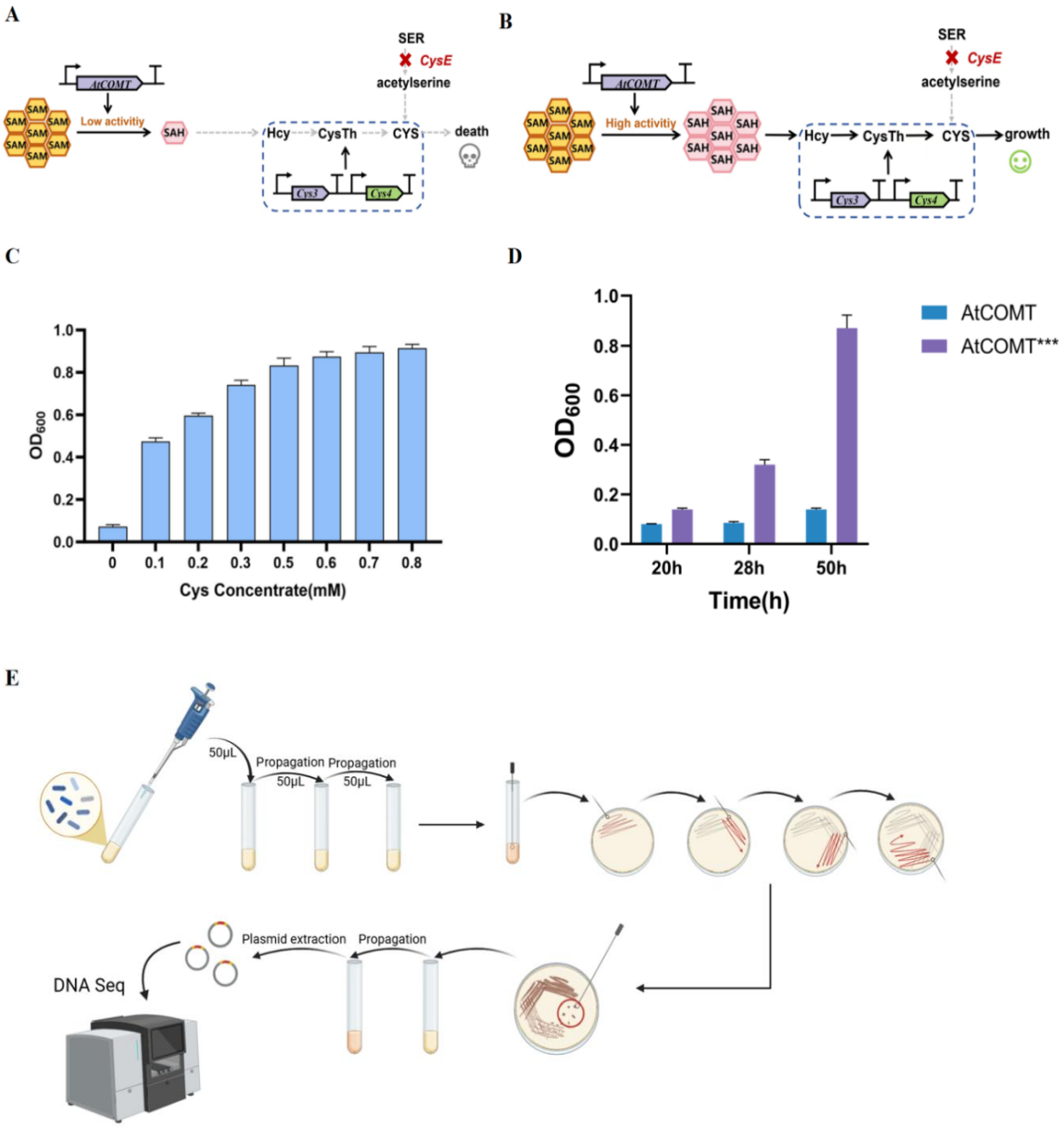

Figure 5. Construction of cysteine auxotrophic whole-cell biosensor and schematic diagram of screening process for AtCOMT mutants.

(A) SAM is converted to SAH by AtCOMT with low activity. SAH further participates in the reaction to generate Hcy, which is then converted to Cys by related enzymes. Meanwhile, Ser cannot generate O-acetylserine due to the inhibition of *CysE*, ultimately leading to cell death due to changes related to Cys and other factors. **(B)** Strains with high enzyme activity catalyze the demethylation of SAM to generate SAH via AtCOMT. Under the functions of genes *Cys3* and *Cys4*, SAH is further converted to Cys, thereby enabling the growth of *CysE* gene-knockout

strains. **(C)** The growth of the strain positively correlated with Cys concentration, demonstrating that the sensor could successfully detect **(D)** The enzymatic activity of AtCOMT was positively correlated with the growth status of the bacteria. **(E)** A 50 μL aliquot was transferred to M9 medium supplemented with exogenous Cys and subjected to transition culture at 30°C for 12 hours. After the bacterial solution became slightly turbid, 250 μL of the bacterial solution was transferred to M9 medium containing SAM and NAS but no cysteine, and this process was repeated once. Then, a bacterial loop was used to take the bacterial solution and streak it on the plate with the corresponding antibiotic resistance. Finally, single colonies were picked for inoculation and plasmid extraction, followed by DNA sequencing.

2.4.3 Selecting Results and Enzymatic Activity Validation

Following two rounds of screening and detection of the reaction product (melatonin, MT) via liquid chromatography, the top-performing colonies were isolated. 38 out of 72 tested clones exhibited higher enzymatic activity than the *AtCOMT**** template **(Figure 6A and 6B)**. To eliminate interference from the helper plasmid pLB1s-*Cys3-Cys4* (in the chassis host) on enzymatic activity measurements, the optimal mutant plasmids from screening were re-transformed into BW25113 wild-type and BWΔ*CysE* strains for validation. Results revealed that after helper plasmid removal, the mutants retained higher enzymatic activity in both genetic backgrounds; notably, the most active AtCOMT mutant K187R-C296F-Q310I-V314T exhibited an approximately 84% increase in enzymatic activity compared to the most catalytic efficient AtCOMT mutants previously reported **(Figure 6C and 6D)**.

The results provided a foundation for subsequent enzymatic mechanism analysis

and molecular simulation.

2.4.4 Molecular Docking Suggests Enhanced Substrate Binding in Improved AtCOMT Mutant

To understand the molecular (and structural) basis for the improved AtCOMT activity, we analyzed molecular docking (and HPLC analyses) on the AtCOMT*** and its highest-performing mutant AtCOMT $^{K187R\text{-}C296F\text{-}Q310I\text{-}V314T}$ **(Figure 6E and 6F)**. The analysis revealed a trade-off between catalytic geometry and binding stability: while the wild-type exhibits a more optimal catalytic geometry, with a shorter distance between His267 N and the substrate NAS reactive site, the mutant shows stronger binding stability, reflected by a lower binding energy (−6.2 vs. −5.9 kcal/mol).

Despite a slight increase in the catalytic distance, the mutation enhances overall catalytic efficiency through significantly improved substrate binding ($\Delta G = -0.3$ kcal/mol). These results imply that the contribution of binding affinity outweighs the minor compromise in of catalytic geometry positioning.

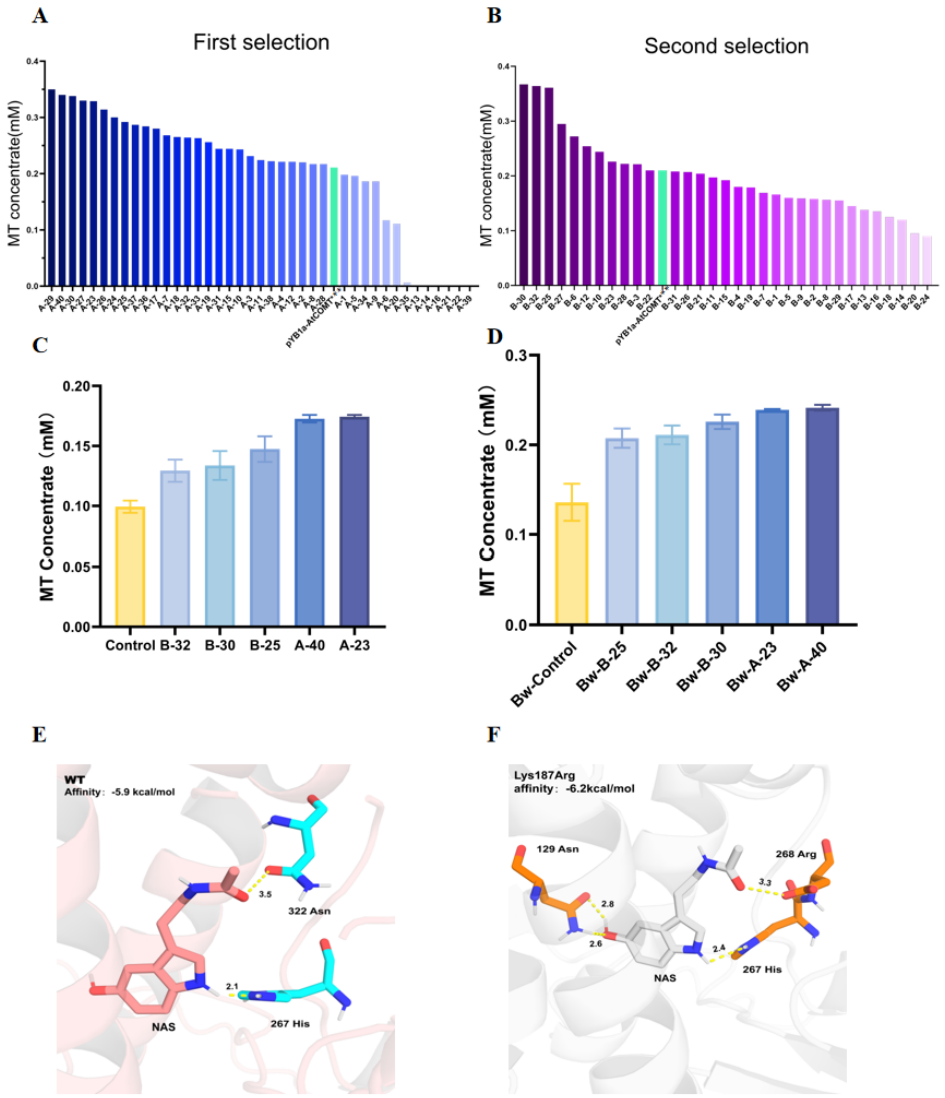

Figure 6. Results of AtCOMT mutant selection and molecular docking results.

(A) Among the 40 bacteria selected for detection in the first round of screening, 27 showed higher (enzymatic activity) than the original AtCOMT*** (labeled in green color). **(B)** Among the 32 bacteria selected for detection in the second round of screening, 11 showed higher (enzymatic activity) than the original AtCOMT*** (labeled in green color). **(C)** The five strains with the highest enzymatic activity from the two rounds of screening were treated to eliminate the pLB1s-*Cys3*-*Cys4* plasmid, and then re-detected in BWΔ*CysE* strain. **(D)** Their enzymatic activities were re-examined in the BW25113 strain background. The results showed that the screened AtCOMT$^{(K187R\text{-}C296F\text{-}Q310I\text{-}V314T)}$ with the highest enzymatic activity exhibited an approximately 84% increase compared to the existing template with the highest enzymatic activity. **(E)** AtCOMT*** Distance between His267 and NE2: 2.1Å, Affinity: -5.9 kcal/mol. **(F)** AtCOMT $^{(K187R\text{-}C296F\text{-}Q310I\text{-}V314T)}$ Distance between

His267 and NE2: 2.4Å, Affinity: -6.2 kcal/mol.

3. Discussion

In this study, the metabolic pathway from glucose to MT was improved by two strategies: optimizing the synthesis and utilization efficiency of L-tryptophan (L-Trp), and modifying AtCOMT via directed evolution. Furthermore, the yield of L-Trp (a precursor of MT) was enhanced through upstream genes knockout and overexpression, whole-genome mutagenesis, and screening using the *tnaC* biosensor. The L-Trp yield reached 3.99 g/L, representing a 1609.9-fold increase compared to the wild-type strain. Second, a high-efficiency screening system for the methyl cycle was constructed; notably, the catalytic efficiency of the screened AtCOMT mutants was approximately 84% higher than that of the previously reported most efficient mutant C296F-Q310L-V314T[11]. We also made site-directed mutation of *aroG* gene according to literature, the L-Trp yield reached 5 g/L, representing a 171-fold increase compared to the wild-type strain[32,33] **(Figure S1)**.

Previous studies have primarily focused on cofactor engineering, whereas t he innovation of this study lies in optimizing the glucose-to-L-Trp metabolic p athway and performing structure-guided modification of AtCOMT. Through rati onal optimization of the L-Trp metabolic pathway, this study demonstrated that

the highest L-Trp yield (3.99 g/L) was achieved when the plasmid pBR322-*trp*^{fbr}*EDCBA-aroG*^{fbr}*-serA*^{fbr} was introduced into the BWΔ*trpR*Δ*tnaAB*Δ*pheA* chassis strain. Subsequently, random mutagenesis was successfully introduced into the BWΔ*trpR*Δ*tnaAB* genome using the MP6 mutant plasmid, resulting in an approximately 3.25 times yield increase relative to the unmutated plasmid. Further analysis of the mutated plasmid revealed that the unique mutations in strain 3-4 are manifested in systemic regulation, which may increase reduction capacity (*ligA*) and degrade competing pathway mRNA (*pnp*); while the mutations in strain 10-7 are related to transport enhancements, capable of facilitating amino acid efflux (*rhtC*) and precursor supply (*tyrR*).

To achieve de novo melatonin production from glucose, future studies will focus on creating a higher-tryptophan chassis. This will be achieved by systematically eliminating metabolic bottlenecks (e.g., *pheA*, *pykA*, *ptsG*, *pykF* knockouts) and applying directed evolution to the *aroG* gene. The optimized chassis and *aroG* variants will be combined to maximize precursor supply before engineering the final melatonin biosynthesis pathway.

4. Materials and Methods

4.1 Chemicals, Strains and Materials

4.1.1 Compounds and Standards

This study focuses on the de novo synthesis pathway of MT in *E. coli*, which involves several key intermediates, including L-trp, 5-HTP, 5-HT, NAS, and MT. All these compounds were purchased from Aladdin Biotechnology Co., Ltd. Other reagents used in the experiment are conventional molecular biology reagents. In this study, a series of melatonin standard solutions with gradient concentrations (0.2mM, 0.4mM, 0.6mM, 0.8mM, 1mM) were prepared and detected by High-Performance Liquid Chromatography (HPLC) to obtain the standard curve of melatonin **(Figure S2)**.

4.1.2 Materials

During the screening process using whole-cell biosensors, strains were cultured in LB medium. The preparation method of LB liquid medium is as follows: dissolve 10 g of tryptone, 5 g of yeast extract, and 10 g of sodium chloride in 1 L of deionized water; for the formulation of LB solid medium, an additional 15 g/L of agar is required to prepare culture plates. During the construction and screening of the mutant library, *E. coli* strains were grown in M9 medium. The components of M9 medium include: 17 g of $Na_2HPO_4 \cdot 7H_2O$, 3 g of KH_2PO_4, 0.5 g of NaCl, 1 g of NH_4Cl, 2 mM of $MgSO_4$, 0.1 mM of $CaCl_2$, and 4 g/L of glucose. All culture conditions were set at 37°C with shaking at 200 rpm, while the culture conditions in 96-well plates were 30°C with shaking at 850 rpm. Streptomycin, chloramphenicol, and kanamycin were used as conventional antibiotics at a working concentration of 100 mg/L. The formulation of ZYM5052

medium is: 10 g/L of tryptone, 5 g/L of yeast extract, 50 mM of phosphate, 50 mM of ammonium chloride, 5 mM of sodium sulfate, 0.5% glycerol, 0.05% glucose, 0.2 mM of magnesium sulfate, and a variety of essential metal ions. The transformation solution was prepared using 50 mM Tris-HCl buffer (pH 9). The competent cells of DH5α, BW25113, and BWΔ*trpR*Δ*tnaAB*Δ*pheA* used in the experiment were prepared in the laboratory, and some competent cells were purchased from Shanghai Weidi Biotechnology Co., Ltd.

4.1.3 Strains

The bacterial strains and plasmids used in this study are listed in **Supplementary Table 2**. All chemicals used in the experiment are of analytical grade and purchased from reliable commercial suppliers. The main strain used is the genetically edited *E. coli* BWΔ*trpR*Δ*tnaAB*Δ*pheA*, and other materials include plasmid vectors for recombinant genes and related components of whole-cell biosensors. The primers used for plasmid construction were synthesized by Ruibiotech (Harbin, China), and detailed information is provided in **Supplementary Table 3**.

4.1.4 Gene Synthesis and Plasmid Construction

Genes including *CrTDC*, *SgAANAT*, *AtCOMT*, *DjTPH*, *phhB*, *Pcd, Dpr, Pts,* and *Spr* were used in this study. All genes were codon-optimized and synthesized by Integrated DNA Technologies (IDT). Plasmid construction was performed using the

Gibson Assembly method (Gibson Assembly, C116), and cloning was completed using the Gibson Assembly Cloning Kit (New England Biolabs, NEB).

To achieve the knockout of *ptsG*, *pykF*, *pykA*, and *pheA* genes in the *E. coli* genome, this study first constructed ptarget-*ptsG*, ptarget-*pheA*, ptarget-*pykF*, and ptarget-*pykA* plasmids. sgRNA was used to guide Cas9 for site-specific cleavage of DNA, and then Donor-U500D500 plasmids were constructed. Using DH5α competent cells as templates, PCR was performed on Donor, U500, and D500 respectively. The PCR products were recovered by gel extraction and subjected to Gibson ligation. Subsequently, the U500D500 targeting fragments of *ptsG*, *pykF*, *pykA*, and *pheA* were prepared respectively for gene knockout. The *pEC-Cas9* plasmid was transformed into *E. coli* BWΔ*trpR*Δ*tnaAB* to prepare electrocompetent cells. 100 μL of competent cells, 300 ng of ptarget-*pykA/pykF/ptsG/pheA* genes, and 500 ng of targeting fragments were incubated on ice for 10-30 minutes, and then electrotransformed into the competent cells. Immediately after electroporation, 1000 μL of LB medium preheated to 37°C was added, gently mixed, and transferred to a 1.5 mL centrifuge tube, followed by incubation in a shaker at 37°C and 150 rpm for 45-60 minutes. After incubation, the cells were spread on double-antibiotic selective plates containing kanamycin (Kana) and streptomycin (Str) for screening. Finally, colony PCR was used to verify the effect of gene knockout.

4.2 Mutant Construction

4.2.1 Genome-Wide Mutation

Using BWΔ*trpR*Δ*tnaAB* as the chassis strain, the plasmids MP6-K, pLB1s-PBAD-*tnaC-mcherry-cmr*, and pYB1a-P23119-*tnaE*^{S40F}*DCBA* were introduced. Induction culture was performed using M9-Y medium (comprising 2 mL of 5×M9, 1 mL of 20% glycerol, 20 μL of $MgSO_4$, 1 μL of $CaCl_2$, 50 μL of 100 g/L yeast extract, 100 μL of L-Ara (L-arabinose), and 4 μL of Cmr (chloramphenicol)).

4.2.2 Random Mutation

Mutants were constructed via the random mutagenesis method. First, the target sequence was selected, and random mutation was conducted on the *AtCOMT**** gene (Arabidopsis thaliana Caffeic acid O-Methyltransferase gene). A mutant library was constructed using error-prone PCR technology. The PCR reaction conditions were set as follows: initial denaturation at 98°C for 5 minutes; followed by 30 cycles, each consisting of denaturation at 98°C for 30 seconds, annealing at 59°C for 30 seconds, and extension at 72°C for 30 seconds; final extension at 72°C for 5 minutes, and subsequent holding at 4°C.

4.2.3 Plasmid Library Construction

The randomly mutated *AtCOMT** gene was ligated with the vector using the

Golden Gate cloning method to construct a mutant library[34]. According to the ratio of 1 μL of plasmid transformed into 100 μL of competent cells, the plasmid library was transformed into 10 strains of *Escherichia coli* BWΔ*CysE*/pLb1s-*Cys3*-*Cys4* to obtain recombinant strains. Referring to the published method[35], the transformed bacterial solution was spread onto 10 LB agar media containing 100 mg/mL antibiotics respectively, and cultured at 37°C for 12 hours. Subsequently, the strains on the 10 media were washed into a 50 mL Erlenmeyer flask using 20 mL of liquid LB medium. The library size of the plasmid library was approximately 30,000 to 50,000 clones.

4.3 Mutant Library Screening

4.3.1 Screening Using Tryptophan Whole-Cell Biosensor

Chloramphenicol (Cmr) was used as the screening antibiotic (with a screening concentration of 12 μg/mL) for the preliminary screening of mutant clone monoclonals, and then high-performance liquid chromatography (HPLC) was employed to verify the high-yield phenotype. In the multi-round fermentation screening process, the mutant strains were inoculated onto LB plates containing antibiotics. Monoclones were picked for expanded culture and then transferred to the seed medium. When the optical density (OD value) of the bacterial solution reached 5–6, the bacterial cells were collected and transferred to the fermentation medium. After culturing at 37°C for 28 hours, samples were taken and analyzed by HPLC.

4.3.2 Screening Using Cysteine Whole-Cell Biosensor

The mutant library was transferred at a 1% inoculation amount into 5 mL of 1×M9 transition medium (including 1 mM M9 basal medium, 0.2 mM cysteine, 2% glycerol, 0.2% arabinose, 0.1 mM calcium chloride, 0.2 mM magnesium sulfate, and antibiotics), and cultured at 30°C with a rotation speed of 200 rpm for 12 hours. Then, it was transferred at a 5% inoculation amount into 5 mL of 1×M9 screening medium (including 1 mM M9 basal medium, 0.2 mM cysteine, 2% glycerol, 0.2% arabinose, 0.1 mM calcium chloride, 0.2 mM magnesium sulfate, 2 mM SAM (S-adenosylmethionine), 1 mM NAS (nicotinic acid), and antibiotics). After the bacterial solution became turbid (indicating massive bacterial proliferation), transfer was performed again. The bacterial solution that had been transferred twice in the screening system was subjected to streak culture, and single colonies were picked for enzyme activity detection using HPLC.

4.4 High-Performance Liquid Chromatography (HPLC) Detection

4.4.1 Sample Preparation

The whole-cell catalytic reaction solution was diluted with sterile water at an appropriate ratio to ensure complete dissolution of the product. Then, 200 μL of the diluted reaction solution was taken and centrifuged at 10,000×g (relative centrifugal force) for 10 minutes. The supernatant after centrifugation was transferred to a new 1.5

mL centrifuge tube, and the supernatant was filtered through a 0.22 μm filter membrane using a 1 mL syringe. The filtrate was collected and loaded into an HPLC vial.

4.4.2 HPLC Detection

An Agilent 1100 Series High-Performance Liquid Chromatograph was used for analysis, with an Agilent XB-C8 column (specifications: 4.6×250 mm², inner diameter 5 μm). The specific detection parameters are as follows:

a. L-Trp (L-tryptophan): The detection wavelength was set to 278 nm; the mobile phase was a mixture of methanol and 0.85 mM potassium dihydrogen phosphate aqueous solution (volume ratio 10:90, v/v); the injection volume was 10 μL; the flow rate was 1 mL/min.
b. 5-HTP (5-hydroxytryptophan), 5-HT (5-hydroxytryptamine), NAS (nicotinic acid): The detection wavelength was 278 nm for all; the mobile phase was a mixture of acetonitrile and 0.025 mM ammonium acetate aqueous solution (volume ratio 10:90, v/v).
c. MT (melatonin): The detection wavelength was set to 278 nm; the mobile phase was a mixture of methanol and water (volume ratio 40:60, v/v).

4.5 Whole-Genome Resequencing and Variant Calling Workflow

4.5.1 Genomic DNA Extraction and Whole-Genome Resequencing

Library preparation and sequencing were performed by Sangon Biotech (Shanghai, China). Paired-end libraries with an insert size of approximately 350 bp were constructed and sequenced on an Illumina NovaSeq platform, generating 150 bp paired-end reads.

4.5.2 Data Quality Control and Variant Calling

The raw sequencing reads were subjected to quality control using FastQC (v0.11.8). Adapters and low-quality bases (Phred score < 20) were trimmed using Trimmomatic (v0.39)[36]. The resulting clean reads were then aligned to the *E. coli* reference genome NZ_CP009273 using the Burrows-Wheeler Aligner (BWA-MEM, v0.7.17)[37].

Duplicates were marked using GATK MarkDuplicates (v4.1.1.0)[38]. Single Nucleotide Polymorphisms (SNPs) and small insertions/deletions (InDels) were called for all three samples simultaneously using the GATK HaplotypeCaller workflow, following the GATK Best Practices. High-confidence variants were filtered based on standard parameters (QD < 2.0, FS > 60.0, MQ < 40.0).

4.5.3 Variant Annotation and Functional Analysis

The functional effects of the identified variants were annotated using SnpEff (v4.3t)7 based on the reference genome annotation. To identify mutations acquired during the adaptive evolution, variants present in the parental WT strain were treated

as background and subtracted from the variant lists of strains '3-4' and '10-7'. Mutations leading to non-synonymous changes (missense, nonsense, frameshift) in coding regions were prioritized for further analysis. The distribution of mutations across the genome was visualized using the circlize R package. The comparison of shared and unique variants among the WT, '3-4', and '10-7' strains was performed and visualized using the EVenn web server[39].

4.5.4 Gene Ontology (GO) and Pathway Enrichment Analysis

To understand the biological implications of the acquired mutations, Gene Ontology (GO) 10 enrichment analysis was performed. The list of genes carrying non-synonymous mutations in the evolved strains ('3-4' and '10-7') was used as the input set. GO term enrichment for Biological Process (BP), Molecular Function (MF), and Cellular Component (CC) categories was conducted. A p-value < 0.05 was considered statistically significant using R package clusterProfiler[40] **(Table. S4)**.

4.6 Molecular Docking Simulation and Analysis Workflow

4.6.1 Homology Modeling and Protein Preparation

The three-dimensional structure of the wild-type 5-O-methyltransferase was modeled using the AlphaFold2[41] protein structure prediction server. For the wild-type protein, the structure was prepared for docking using AutoDockTools (v1.5.6). This

process involved removing all water molecules and adding polar hydrogen atoms to the protein structure.

For the mutant protein structure, which contained the K187R, an energy minimization step was performed prior to docking preparation using GROMACS (v2021.4)[42]. The system was minimized using a combination of the steepest descent and conjugate gradient algorithms until the maximum force (Fmax) on any atom was less than 50 $kJ \cdot mol^{-1} \cdot nm^{-1}$. After minimization, the mutant structure was prepared in the same manner as the wild-type using AutoDockTools, with water molecules removed and polar hydrogens added.

4.6.2 Molecular Docking Simulation

Molecular docking simulations were performed to investigate the binding of N-Acetylserotonin to both the wild-type and mutant proteins. The docking calculations were carried out using AutoDock Vina (v1.2.3)[43]. The search space (grid box) was centered on the predicted active site of the protein. The exhaustiveness parameter was set to 9 to ensure a thorough conformational search. For each docking run, the top-scoring binding pose, based on the Vina score (kcal/mol), was selected for further analysis.

4.6.3 Visualization and Analysis

The resulting protein-ligand complexes were visualized and analyzed using

PyMOL.

Declaration of competing interest

The authors declare no competing interests.

Acknowledgments

This research was supported by funding from Northeast Forestry University. We sincerely thank the strong support from the College of Life Sciences and the Aulin College, Northeast Forestry University. We are grateful for the experimental platform provided by the university, the guidance of our teachers, and the assistance of our mentors.

References

1. Wang, L., Deng, Y., Gao, J. et al. Biosynthesis of melatonin from l-tryptophan by an engineered microbial cell factory. *Biotechnol Biofuels* 17, 27 (2024).

DOI: https://doi.org/10.1186/s13068-024-02476-7

2. Sun, C., Liu, L., Wang, L., Li, B., Jin, C., and Lin, X. Melatonin: A master regulator of plant development and stress responses. *Journal of Integrative Plant Biology.* 63, 126–145 (2021).

DOI: https://doi.org/10.1111/jipb.12993

3. Megha, K. B., Arathi, A., Shikha, S., Alka, R., Ramya, P., and Mohanan, P. V. Significance of Melatonin in the Regulation of Circadian Rhythms and Disease Management. *Molecular Neurobiology.* 61, 5541–5571 (2024).

DOI: https://doi.org/10.1007/s12035-024-03915-0

4. Xie, X., Ding, D., Bai, D., Zhu, Y., Sun, W., Sun, Y., and Zhang, D. Melatonin biosynthesis pathways in nature and its production in engineered microorganisms. *Synthetic and Systems Biotechnology.* 7, 544–553 (2022).

DOI: https://doi.org/10.1016/j.synbio.2021.12.011

5. He, L., Li, J. L., Zhang, J. J., Su, P., & Zheng, S. L. Microwave Assisted Synthesis of Melatonin. *Synthetic Communications.* 33, 741–747 (2003).

DOI: https://doi.org/10.1081/SCC-120016317

6. Meng, X., Li, Y., Li, S. et al. Dietary Sources and Bioactivities of Melatonin. *Nutrients* 9, 367 (2017).

DOI: https://doi.org/10.3390/nu9040367

7. Luo, H., Schneider, K., Christensen, U., Lei, Y., Herrgard, M., and Palsson, B. Ø. Microbial Synthesis of Human-Hormone Melatonin at Gram Scales. *ACS Synthetic*

Biology. 9, 1240–1245 (2020).

DOI: https://doi.org/10.1021/acssynbio.0c00065

8. Zimmermann, P., Kurth, S., Pugin, B. et al. Microbial melatonin metabolism in the human intestine as a therapeutic target for dysbiosis and rhythm disorders. *npj Biofilms Microbiomes* 10, 139 (2024).

DOI: https://doi.org/10.1038/s41522-024-00605-6

9. Li, G., & Young, K. D. (2013). Indole production by the tryptophanase TnaA in *Escherichia coli* is determined by the amount of exogenous tryptophan. Microbiology, 159(Pt_2), 402-410.

DOI : https://doi.org/10.1099/mic.0.064139-0

10. Morgan, J. (2020). Combining random mutagenesis and metabolic engineering for enhanced tryptophan production in Synechocystis sp. strain PCC 6803. Applied and environmental microbiology, 86(9), e02816-19

DOI: https://doi.org/10.1128/AEM.02816-19

11. Wang, W., Su, S., Wang, S., Ye, L., and Yu, H. Significantly improved catalytic efficiency of caffeic acid O-methyltransferase towards N-acetylserotonin by

strengthening its interactions with the unnatural substrate's terminal structure. *Enzyme and Microbial Technology.* 125, 1–5 (2019).

DOI : https://doi.org/10.1016/j.enzmictec.2019.02.005

12. Chen, J., Wang, Y., Zheng, P., & Sun, J, Engineering synthetic auxotrophs for growth-coupled directed protein evolution. Trends in Biotechnology, 40(7), 773 – 776, (2022).

DOI: https://doi.org/10.1016/j.tibtech.2022.01.010

13. Williams, T. C., Pretorius, I. S., & Paulsen, I. T., Synthetic Evolution of Metabolic Productivity Using Biosensors. Trends in Biotechnology, 34(5), 371 – 381,(2016).

DOI : https://doi.org/10.1016/j.tibtech.2016.02.002

14. Khosla, C.; Luo, H.; Hansen, A. S. L.; Yang, L.; Schneider, K.; Kristensen, M.; Christensen, U.; Christensen, H. B.; Du, B.; Özdemir, E.; et al. Coupling S-adenosylmethionine–dependent methylation to growth: Design and uses. PLOS Biology 2019, 17 (3).

DOI: https://doi.org/10.1371/journal.pbio.2007050

15. Ding, D., Bai, D., Li, J., Mao, Z., Zhu, Y., Liu, P., Lin, J., Ma, H., & Zhang, D.

(2021). Analyzing the genetic characteristics of a tryptophan-overproducing Escherichia coli. Bioprocess and Biosystems Engineering, 44(8), 1685–1697.

DOI : https://doi.org/10.1007/s00449-021-02552-4

16. Gu, P., Yang, F., Kang, J., Wang, Q., & Qi, Q. (2012). One-step of tryptophan attenuator inactivation and promoter swapping to improve the production of L-tryptophan in *Escherichia coli.* Microbial cell factories, 11(1),30.

DOI : https://doi.org/10.1186/1475-2859-11-30

17. Yao, R., Hirose, Y., Sarkar, D., Nakahigashi, K., Ye, Q., & Shimizu, K. (2011). Catabolic regulation analysis of *Escherichia coli* and its crp, mlc, mgsA, pgi and ptsG mutants. Microbial Cell Factories, 10(1), 67.

DOI : https://doi.org/10.1186/1475-2859-10-67

18. Liu, L., Chen, S., & Wu, J. (2017). Phosphoenolpyruvate: glucose phosphotransferase system modification increases the conversion rate during L-tryptophan production in *Escherichia coli.* Journal of Industrial Microbiology and Biotechnology, 44(10), 1385-1395.

DOI : https://doi.org/10.1007/s10295-017-1959-3

19. Chen, Y., Liu, Y., Ding, D., Cong, L., & Zhang, D. (2018). Rational design and analysis of an *Escherichia coli* strain for high-efficiency tryptophan production. Journal of Industrial Microbiology and Biotechnology, 45(5), 357-367.

DOI : https://doi.org/10.1007/s10295-018-2020-x

20. Liu, X., Niu, H., Huang, Z., Li, Q., & Gu, P. (2020). Construction of a switchable synthetic *Escherichia coli.* for aromatic amino acids by a tunable switch. Journal of Industrial Microbiology and Biotechnology, 47(2), 233-242.

DOI : https://doi.org/10.1007/s10295-020-02262-y

21. Liu, Y., Yuan, H., Ding, D., Dong, H., Wang, Q., & Zhang, D., Establishment of a Biosensor-based High-Throughput Screening Platform for Tryptophan Overproduction. ACS Synthetic Biology, 10(6), 1402–1411, (2021).

DOI: https://doi.org/10.1021/acssynbio.0c00647

22. Badran, A., Liu, D., Development of potent in vivo mutagenesis plasmids with broad mutational spectra. Nat Commun 6, 8425, (2015).

DOI: https://doi.org/10.1038/ncomms9425

23. Ding, D., Bai, D., Li, J., Mao, Z., Zhu, Y., Liu, P., Lin, J., Ma, H., & Zhang, D.

(2021). Analyzing the genetic characteristics of a tryptophan-overproducing *Escherichia coli.* Bioprocess and Biosystems Engineering, 44(8), 1685–1697.

DOI: https://doi.org/10.1007/s00449-021-02552-4

24. Chauleau, M., & Shuman, S. (2016). Kinetic mechanism and fidelity of nick sealing by *Escherichia coli*. NAD+-dependent DNA ligase (LigA). Nucleic acids research, 44(5), 2298–2309.

DOI: https://doi.org/10.1093/nar/gkw049

25. Shi, Z., Yang, W. Z., Lin-Chao, S., Chak, K. F., & Yuan, H. S. (2008). Crystal structure of *Escherichia coli.* PNPase: central channel residues are involved in processive RNA degradation. RNA (New York, N.Y.), 14(11), 2361–2371.

DOI: https://doi.org/10.1261/rna.1244308

26. Diesveld, R., Tietze, N., Fürst, O., Reth, A., Bathe, B., Sahm, H., & Eggeling, L. (2009). Activity of exporters of *Escherichia coli* in Corynebacterium glutamicum, and their use to increase L-threonine production. Journal of molecular microbiology and biotechnology, 16(3-4), 198–207.

DOI: https://doi.org/10.1159/000142530

27. Verger, D., Carr, P. D., Kwok, T., & Ollis, D. L. (2007). Crystal structure of the N-terminal domain of the TyrR transcription factor responsible for gene regulation of aromatic amino acid biosynthesis and transport in *Escherichia coli* K12. Journal of molecular biology, 367(1), 102–112.

DOI: https://doi.org/10.1016/j.jmb.2006.12.018

28. Kowlessur D , Kaufman S .Cloning and expression of recombinant human pineal tryptophan hydroxylase in *Escherichia coli*: purification and characterization of the cloned

DOI: https://doi.org/10.1016/S0167-4838(99)00184-3

29. Park S, Kang K, Lee SW, Ahn MJ, Bae JM, Back K. Production of serotonin by dual expression of tryptophan decarboxylase and tryptamine 5-hydroxylase in *Escherichia coli.* Appl Microbiol Biotechnol. 2011;89(5):1387-1394.

DOI: https://doi.org/10.1007/s00253-010-2994-4

30. Deloménie C, Fouix S, Longuemaux S, et al. Identification and functional characterization of arylamine N-acetyltransferases in eubacteria: evidence for highly selective acetylation of 5-aminosalicylic acid. J Bacteriol. 2001;183(11):3417-3427.

DOI: https://doi.org/10.1128/JB.183.11.3417-3427.2001

31. Byeon Y, Lee HJ, Lee HY, Back K. Cloning and functional characterization of the Arabidopsis N-acetylserotonin O-methyltransferase responsible for melatonin synthesis. J Pineal Res. 2016;60(1):65-73.

DOI: https://doi.org/10.1111/jpi.12289

32. Chen M, Ma C, Chen L, et al.Integrated laboratory evolution and rational engineering of GalP/Glk-dependent *Escherichia coli* for higher yield and productivity of L-tryptophan biosynthesis[J]. Metabolic Engineering Communications,2021,12e00167-e00167.

DOI : https://dx.doi.org/10.1007/S43393-025-00338-3

33. Hou M, Gao S, Wu J, et al. Metabolic engineering of *Escherichia co*li to enhance L-tryptophan biosynthesis[J]. Systems Microbiology and Biomanufacturing,2025,5(2) : 1-13.

DOI : https://dx.doi.org/10.1016/J.MEC.2021.E00167

34. Engler, C., & Marillonnet, S, Golden Gate cloning. Methods in Molecular Biology, 119–131, (2013).

DOI : https://doi.org/10.1007/978-1-62703-764-8

35. Froger, A., & Hall, J. E, Transformation of Plasmid DNA into *E. coli* Using the Heat Shock Method. Journal of Visualized Experiments, 6, (2007).

DOI: https://doi.org/10.3791/253

36. Bolger, A. M., Lohse, M., & Usadel, B. (2014). Trimmomatic: a flexible trimmer for Illumina sequence data. Bioinformatics (Oxford, England), 30(15), 2114–2120.

DOI：https://doi.org/10.1093/bioinformatics/btu1702

37. Li, H. (2013). Aligning sequence reads, clone sequences and assembly contigs with BWA-MEM [Preprint]. arXiv.

DOI：https://arxiv.org/abs/1303.3997

38. McKenna, A., Hanna, M., Banks, E., Sivachenko, A., Cibulskis, K., Kernytsky, A., Garimella, K., Altshuler, D., Gabriel, S., Daly, M., & DePristo, M. A. (2010). The Genome Analysis Toolkit: a MapReduce framework for analyzing next-generation DNA sequencing data. Genome research, 20(9), 1297–1303.

DOI：https://doi.org/10.1101/gr.107524.110

39. Yang, M., Chen, T., Liu, Y. X., & Huang, L. (2024). Visualizing set relationships:

EVenn's comprehensive approach to Venn diagrams. iMeta, e184.

DOI: https://doi.org/10.1002/imt2.184

40. Yu, G., Wang, L. G., Han, Y., & He, Q. Y. (2012). clusterProfiler: an R package for comparing biological themes among gene clusters. Omics : a journal of integrative biology, 16(5), 284–287.

DOI : https://doi.org/10.1089/omi.2011.0118

41. Jumper, J., Evans, R., Pritzel, A., Green, T., Figurnov, M., Ronneberger, O. et al. (2021). Highly accurate protein structure prediction with AlphaFold. nature, 596(7873), 583-589.

DOI: https://doi.org/10.1038/s41586-021-03819-2

42. Abraham, M. J., Murtola, T., Schulz, R., Páll, S., Smith, J. C., Hess, B., & Lindahl, E. (2015). GROMACS: High performance molecular simulations through multi-level parallelism from laptops to supercomputers. SoftwareX, 1, 19-25.

DOI: https://doi.org/10.1016/j.softx.2015.06.001

43. Eberhardt, J., Santos-Martins, D., Tillack, A. F., & Forli, S. (2021). AutoDock Vina 1.2. 0: new docking methods, expanded force field, and python bindings. Journal of

chemical information and modeling, 61(8), 3891-3898.

DOI：https://doi.org/10.1021/acs.jcim.1c00203